

# Journal of Materials Chemistry A

Accepted Manuscript



This is an *Accepted Manuscript*, which has been through the Royal Society of Chemistry peer review process and has been accepted for publication.

*Accepted Manuscripts* are published online shortly after acceptance, before technical editing, formatting and proof reading. Using this free service, authors can make their results available to the community, in citable form, before we publish the edited article. We will replace this *Accepted Manuscript* with the edited and formatted *Advance Article* as soon as it is available.

You can find more information about *Accepted Manuscripts* in the [Information for Authors](#).

Please note that technical editing may introduce minor changes to the text and/or graphics, which may alter content. The journal's standard [Terms & Conditions](#) and the [Ethical guidelines](#) still apply. In no event shall the Royal Society of Chemistry be held responsible for any errors or omissions in this *Accepted Manuscript* or any consequences arising from the use of any information it contains.

## An insight into surface segregation and chromium deposition on

### $\text{La}_{0.6}\text{Sr}_{0.4}\text{Co}_{0.2}\text{Fe}_{0.8}\text{O}_{3-\delta}$ cathodes of solid oxide fuel cells

Ling Zhao,<sup>1</sup> John Drennan,<sup>2</sup> Chun Kong,<sup>3</sup> Sudath Amarasinghe,<sup>4</sup> San Ping Jiang<sup>1,\*</sup>

<sup>1</sup>Fuels and Energy Technology Institute & Department of Chemical Engineering,

Curtin University, Perth, WA 6102, Australia

<sup>2</sup>Centre for Microscopy and Microanalysis, University of Queensland, Brisbane, Qld

4072, Australia

<sup>3</sup>Mark Wainright Analytical Centre, University of New South Wales, Sydney, NSW,

Australia

<sup>4</sup>Ceramic Fuel Cells Ltd., Nobel Park, Vic. 3174, Australia

#### Abstract

$\text{La}_{0.6}\text{Sr}_{0.4}\text{Co}_{0.2}\text{Fe}_{0.8}\text{O}_{3-\delta}$ , (LSCF) perovskite oxide is one of the most important cathode materials in the development of intermediate temperature solid oxide fuel cells (IT-SOFCs), but vulnerable to the chromium deposition and poisoning in the presence of gaseous chromium species from chromia-forming metallic interconnect. Despite the extensive studies on Cr deposition on SOFC cathode materials, there is lack of direct evidences on the surface chemistry and Cr deposition. Here, the fundamental relationship between the surface segregation and Cr deposition of LSCF cathodes is studied on dense LSCF bar samples using a dual beam high resolution focused ion beam (FIB) and a high resolution scanning electron microscope coupled with EDS. FIB-EDS mapping results clearly indicate the segregation of SrO and  $\text{Co}_3\text{O}_4$  particles on the LSCF surface after annealing at 800 °C for 96 h. Cr deposition

occurs preferentially on the segregated SrO but not on  $\text{Co}_3\text{O}_4$ . The fundamental reason for the selective and preferential Cr deposition on the segregated SrO is due to the exclusion effect of the presence of SrO on the reactivity between gaseous Cr species and segregated  $\text{Co}_3\text{O}_4$ , inhibiting the Cr deposition on the segregated  $\text{Co}_3\text{O}_4$  particles.

**Keywords:** solid oxide fuel cells; LSCF; strontium and cobalt segregation; selective chromium deposition; exclusion effect; FIB-EDS.

## 1. Introduction

Solid oxide fuel cell (SOFC) is the most efficient technology for the conversion of chemical energy of fuels such as hydrogen and methane directly into electrical power. SOFC traditionally operates at temperatures of 900-1000°C. However, lowering the operation temperature of SOFCs to intermediate temperature range of 600–800 °C not only significantly improves materials' compatibility for the SOFCs, but also reduces the production costs of the SOFC systems.<sup>1, 2</sup> One of the main challenges in the development of intermediate temperature SOFCs or IT-SOFCs is the high polarization losses associated with the cathode materials where the  $\text{O}_2$  reduction reaction takes place.<sup>3-5</sup> There are extensive research activities and efforts in the development of high performance cathode materials for IT-SOFCs. In the intermediate temperature range, mixed ionic and electronic conducting (MIEC)  $(\text{LaSr})(\text{CoFe})\text{O}_{3-\delta}$  (LSCF) perovskite oxides have significantly higher electrochemical activity for the  $\text{O}_2$  reduction reaction and higher oxygen ion conductivity than the

conventional (LaSr)MnO<sub>3</sub> (LSM) cathode.<sup>6-14</sup> LSCF also has low thermal expansion coefficient as compared to other MIEC oxides such as (SmSr)CoO<sub>3-δ</sub> (SSC), (BaSr)(CoFe)O<sub>3-δ</sub> (BSCF) and LnBaCo<sub>2</sub>O<sub>5+δ</sub> (LBCO),<sup>15-18</sup> making it thermally more compatible with ceria-based electrolytes.

From the view of practical application for SOFC stack, metallic interconnect materials are preferred due to their high electronic conductivity, good mechanical property, high thermal conductivity, easy workability and low cost, as compared to the ceramic interconnect materials.<sup>19-21</sup> Up to now, chromia-forming alloys are the most commonly used metallic interconnect materials due to the formation of the conductive chromia scale on the alloy surface under SOFC operating conditions.<sup>20-24</sup> However, on the cathode side, chromium oxide, Cr<sub>2</sub>O<sub>3</sub>, reacts with oxygen in air, forming various gaseous hexavalent chromium species such as CrO<sub>3</sub> and CrO<sub>2</sub>(OH)<sub>2</sub> under the operating temperatures of SOFCs.<sup>25, 26</sup> It has been well known that deposition and poisoning of gaseous Cr species can cause rapid electrochemical performance degradation of cathodes, such as LSM,<sup>27, 28</sup> BSCF<sup>29, 30</sup> and LSCF.<sup>28, 31, 32</sup> Fundamental understanding of the mechanism of the Cr deposition and poisoning of the cathode materials is critical for the development of Cr-tolerant cathodes or better preventive measures to enhance the long-term stability of SOFCs.<sup>33-35</sup>

However, despite the extensive studies on the Cr deposition and poisoning processes, there are still considerable disagreements on the mechanism of the Cr deposition process on the cathodes and its effect on the O<sub>2</sub> reduction reaction.<sup>36</sup> There are two schools of thoughts on the mechanism of Cr deposition. Hilpert et al.<sup>25</sup>

discussed the thermodynamics of the volatile Cr species and showed that the electrochemical reduction of the high valence Cr species and the O<sub>2</sub> reduction reaction are thermodynamic compatible under the SOFC operation conditions. Badwal *et al.*<sup>37</sup> studied SOFC stacks operated between 900 and 1000°C in air/H<sub>2</sub> using a chromia-forming alloy (Plansee) as interconnect. Cell performance declined rapidly and manganese chromium spinel, (Mn,Cr)<sub>3</sub>O<sub>4</sub>, was observed in the LSM cathode. The deposition of Cr is considered to be driven by the electrochemical reduction of gaseous Cr species to solid Cr<sub>2</sub>O<sub>3</sub> phase at the electrode/electrolyte interface in competition with the O<sub>2</sub> reduction reaction.<sup>27,37-42</sup>

We did detailed and systematic studies of the chromium deposition on different SOFC cathodes including LSM,<sup>43-45</sup> LSM/YSZ,<sup>46</sup> LSCF,<sup>31, 47</sup> BSCF,<sup>29, 30</sup> (La,Sr,Ba)(Co,Fe)O<sub>3</sub> (LSBCF).<sup>48,49</sup> The results show that at the initial stages of the O<sub>2</sub> reduction reaction in the presence of a Fe-Cr alloy interconnect, Cr deposition does not occur preferentially at the three phase boundaries at the LSM electrode/YSZ electrolyte interface region, and the deposition of Cr species is random, simply filling the space between the LSM grains with the increase in the cathodic polarization time.<sup>44</sup> Cr deposition is kinetically initiated by manganese species in the electrode/electrolyte interface region. This is also supported by Wang and Fergus<sup>50</sup> in a study of the Cr deposition at a Pt electrode on undoped and Mn-doped YSZ electrolyte, showing a significantly higher Cr deposition on the Mn-doped YSZ electrolyte surface. This indicates that the presence of manganese species promotes the Cr deposition. The formation of manganese nucleation species is closely related to

the oxygen reduction process on the LSM cathodes.<sup>43, 44, 51</sup> In the case of LSCF cathode, Cr deposition occurs predominantly on the surface of the LSCF cathode, forming  $\text{SrCrO}_4$ .<sup>31, 52</sup> Studies also indicate that Ba and Sr segregation plays an important role in the Cr deposition and poisoning on LSCF and BSCF cathodes.<sup>29-31</sup> Chromium deposition at SOFC cathodes is most likely dominated by the chemical reduction of high valence Cr species, facilitated by the nucleation agents on the electrode and electrolyte surface and/or at the electrode/electrolyte interface. However, it appears that there is a lack of direct evidences on the surface segregation and Cr deposition under SOFC operating conditions.

In this work, in order to identify the intrinsic relationship between the surface segregation and the chromium deposition on LSCF electrode materials, we used dense LSCF bar samples instead of conventional porous electrodes. The dense samples would provide a much better platform for the observation of changes of the surface morphology and microstructure by conventional microscopy techniques such as SEM and EDS, as compared to that on porous samples.<sup>53</sup> The results indicate that the strontium and cobalt are segregated on LSCF surface after annealing at 800 °C for 96 h and Cr deposition occurs preferentially on the segregated SrO particles. The oxide couple study provides additional evidences for the selective and preferential nature of Cr deposition on the LSCF cathode materials.

## 2 Experimental

LSCF ( $\text{La}_{0.6}\text{Sr}_{0.4}\text{Co}_{0.2}\text{Fe}_{0.8}\text{O}_{3-\delta}$ , Fuel Cell Materials) powders were pressed into a rectangular bar at 300 MPa, and then sintered at 1350 °C for 5 h in air to form dense

LSCF bar samples. The sintered samples had dimensions of 25 mm × 6.6 mm × 0.62 mm. Cr<sub>2</sub>O<sub>3</sub> powders were placed in an alumina boat. LSCF bar sample and Cr<sub>2</sub>O<sub>3</sub> powder boat were placed side by side in a close-end quartz tube in a furnace and there was no direct contact between the LSCF bar samples and Cr<sub>2</sub>O<sub>3</sub> powder. Thus, deposition of Cr species can only take place through gas phase transportation. The effect of dry and humidified air (3% H<sub>2</sub>O) on the Cr deposition was studied at 800 °C for 96 h. The total gas flow rate was maintained at 50 ml min<sup>-1</sup>. Both freshly prepared and LSCF bar samples heat-treated in the absence of Cr<sub>2</sub>O<sub>3</sub> powders at 800°C for 96 h were used as the references for the study.

The XRD analysis was carried out on a Bruker D8 Advances X-ray diffractometer using Cu Ka radiation generated at 40 kv and 30 mA. Scanning Electron Microscopy (SEM) and Energy Dispersive Spectrometer (EDS) were obtained using a Zesis EVO 40XVP with 15 KeV. Mapping of EDS lasted for 1200 s with 20 KeV. The cross-section of selected regions on the samples was prepared and analyzed by a dual beam high resolution focused ion beam (Ga FIB) and a high resolution scanning electron microscope coupled with EDS (xT Nova NanoLab 200).

In order to study the reaction activity between Cr<sub>2</sub>O<sub>3</sub>, SrO and Co<sub>3</sub>O<sub>4</sub>, different oxide couples were prepared by mixing oxides of Cr<sub>2</sub>O<sub>3</sub>, SrO and Co<sub>3</sub>O<sub>4</sub>. In the case of binary oxide couples, the molar ratio is 1:1 and in the case of ternary oxide couples, two different molar ratios were used, Cr-poor Sr:Co:Cr=1:1:0.25 and Cr-rich Sr:Co:Cr=1:1:4. The oxide couples were thoroughly mixed, followed by calcination at 800 °C for 2 h. In the case of Sr:Co:Cr=1:1:4, the oxide couple was also mixed using

sol-gel method. In this method, stoichiometric amounts of  $\text{Sr}(\text{NO}_3)_2$ ,  $\text{Co}(\text{NO}_3)_2 \cdot 6\text{H}_2\text{O}$  and  $\text{Cr}(\text{NO}_3)_3 \cdot 9\text{H}_2\text{O}$  (all from Sigma-Aldrich) were dissolved and mixed in water, and then agents of EDTA and citric acid at the mole ratio of total metal ions: EDTA: citric acid=1:1.5:1 were added. The pH of the solution was controlled at 7 with the assistance of  $\text{NH}_3 \cdot \text{H}_2\text{O}$ . The solution was then heated till self-combustion occurred. The as-synthesized sol-gel powders were subsequently calcined under the same conditions as the oxide couple mixed by solid state oxides. The phases of the oxide couples after the heat treatment were identified by XRD.

### 3 Results and discussion

#### 3.1. Surface segregation of LSCF in the absence of $\text{Cr}_2\text{O}_3$

Figure 1 is the XRD patterns of the surface of LSCF bar samples with and without the presence of  $\text{Cr}_2\text{O}_3$  at 800 °C for 96 h. Sharp XRD peaks reflect a well-developed crystallization and all the peaks can be indexed as a rhombohedral perovskite structure. The lattice parameters  $a$  and  $c$  were calculated as 5.493 Å and 13.32 Å, close to that reported by Kostogloudis et al.<sup>54</sup> and Waller et al.<sup>55</sup> XRD patterns of LSCF surface after 96 h test under chromium poisoning in both dry and wet air are similar to the LSCF sintered at the same temperature in the absence of chromium oxides. No peaks attributable to other phases can be detected, suggesting the main phase is still the perovskite structure. There is a shift of the XRD peak of LSCF to the low angle, indicating the increase in the lattice parameter of LSCF. Introduction of A-site deficiency into  $\text{La}_{0.6}\text{Sr}_{0.4}\text{Co}_{0.2}\text{Fe}_{0.8}\text{O}_{3-\delta}$  oxides could create additional oxygen vacancies, leading to the increase in the lattice parameters.<sup>54, 56</sup>

Zhou et al. showed that introduction of B-site deficiency into  $\text{Ba}_{0.5}\text{Sr}_{0.5}\text{Co}_{0.8}\text{Fe}_{0.2}\text{O}_{3-\delta}$  also produces additional oxygen vacancies and increases the lattice parameters.<sup>57</sup> Using in situ XRD during SOFC operation conditions (750 °C in  $\text{H}_2/\text{air}$ ), Hardy et al observed the continuous and gradual lattice expansion of LSCF cathodes.<sup>58</sup> The lattice parameters of LSCF samples annealed in the presence of  $\text{Cr}_2\text{O}_3$  at 800°C for 96 h are listed in Table 1.

Figure 2 is the SEM micrographs of the freshly-prepared LSCF and LSCF samples after heat treated at 800 °C in the absence of  $\text{Cr}_2\text{O}_3$  in air for 96 h. The surface of freshly prepared LSCF sample before test is very dense, smooth and clean with no pin holes (Fig.2a). The grain size is in the range of 2 to 11  $\mu\text{m}$ . The large grains of the LSCF samples is clearly due to the high sintering temperature used in this study (1350 °C). EDS analysis indicates that there is no visible differences in the element distribution on large and small grains (Fig.2f). However, the surface morphology of LSCF samples after heat-treatment for 96 h changes significantly (Fig.2c). There is formation of large dark colored particles as large as  $\sim 2 \mu\text{m}$  on the surface of LSCF sample (Fig.2c and d). Majority of the dark colored particles are isolated and located at the grain boundary region though some of them are on the surface of the LSCF grains. The particles have very different crystalline domain or facets as compared to the surrounding LSCF grains (Fig.2e for the particle as circled in (d)), indicating the particles are segregated out of the LSCF perovskite structure. EDS mapping as shown in next section indicates that the isolated and large particles are  $\text{Co}_3\text{O}_4$ . In addition, submicron particles were also formed on the surface of LSCF

grains after annealing (arrows in Fig.2d). Oh et al also reported the observation of the formation of submicron particles on LSCF surface after heat treatment in the temperature range of 600-900°C.<sup>59</sup>

The composition of the segregated particles on LSCF surface after heat treated at 800 °C in the absence of Cr<sub>2</sub>O<sub>3</sub> in air for 96 h was analyzed by EDS mapping, as shown in Fig.3. The LSCF surface is characterized by large number of submicron particles with diameter less than 0.8 μm and one isolated particle as large as 2.7 μm. The EDS mapping shows that the composition of the submicron sized particles is very different from that of the isolated and micron-sized particle. The micron-sized particle is cobalt-rich while the fine and submicron sized particles are strontium-rich. This indicates that both cobalt and strontium are segregated out of the LSCF perovskite structure, forming separated Co- and Sr-rich particles. The formation of much larger Co-rich particles appears to indicate that migration of segregated cobalt species is more facile on the LSCF surface as compared to the segregated Sr. Sr is a firm divalent cation and the Sr enrichment could result in phase separation producing SrO on the surface.<sup>60-62</sup> The observation of Sr segregation on LSCF after annealing in dry air for 96 h is in a good agreement with that reported in the literature.<sup>59, 63</sup> In the case of Co segregation, Baumann et al.<sup>64</sup> observed Co-rich phase on the surface of dense La<sub>0.6</sub>Sr<sub>0.4</sub>Co<sub>0.8</sub>Fe<sub>0.2</sub>O<sub>3-δ</sub> microelectrodes (~100 nm thickness by 20–100 μm diameter) after cathodic polarization at 750 °C in addition to Sr segregation, using X-ray photoelectron spectroscopy (XPS) technique. Liu et al. studied the Raman spectrum of LSCF after long-term test and observed a typical Raman characteristic peak of 675

$\text{cm}^{-1}$ , which was attributed to the  $\text{Co}_3\text{O}_4$  segregated on the LSCF surface.<sup>65</sup> The segregated Co-rich particles most likely exist as  $\text{Co}_3\text{O}_4$ , as at high temperatures,  $\text{Co}_3\text{O}_4$  is probably the most stable form.<sup>66</sup> Recent Raman study indicates that segregated cobalt exists as  $\text{Co}_3\text{O}_4$ .<sup>67</sup>

### 3.2 Cr deposition and surface segregation on LSCF

Figure 4 is the SEM pictures of the LSCF sample after heat-treatment in the presence of  $\text{Cr}_2\text{O}_3$  in dry and wet air for 96 h. In the presence of  $\text{Cr}_2\text{O}_3$  powder, the small particles on the LSCF surface grow significantly and majority of particles are in the range of  $\sim 1.1 \mu\text{m}$  (Fig.4a). After heat-treatment in the presence of  $\text{Cr}_2\text{O}_3$  in wet air, the change in the morphology of LSCF grains becomes clearly visible (Fig.4b). In addition to the formation of large number of small particles on the surface, the surface of LSCF grains is no longer smooth and characterized by the formation of nano-pores or pinholes. This indicates that both gaseous Cr species and moisture accelerate the surface segregation processes and are detrimental to the microstructure of LSCF.

In order to identify the relationship between the segregated Sr- and Co-rich particles and Cr deposition, a FIB-EDS mapping was used to analyze selected particles on the LSCF surface after heat-treatment in the presence of  $\text{Cr}_2\text{O}_3$ . Figure 5 is the typical EDS layer image of an isolated large particle segregated on the LSCF surface after heat-treatment in the presence of  $\text{Cr}_2\text{O}_3$  in dry air at  $800^\circ\text{C}$  for 96 h. The diameter of the particle is  $\sim 3 \mu\text{m}$  and most interesting, it is noted that in the bulk of the particles mainly contains Co (70 wt%) but no Cr (Fig.5c). This is also confirmed by the dominant Co peak in the EDS spectrum of the particle and Cr was not detected

(Fig.5b). This indicates the segregated large particles on the surface of LSCF grains are  $\text{Co}_3\text{O}_4$  and have a very low activity toward gaseous Cr species, in another words, the segregated  $\text{Co}_3\text{O}_4$  does not induce the Cr deposition.

On the same LSCF sample, the FIB-EDS mapping on the much smaller or submicron sized particles confirms the high content of Sr (see Fig.6). Though the EDS mapping does not show clearly Cr enrichment probably due to the small size of the particles (0.2-0.3  $\mu\text{m}$ , see Fig.6c), but the EDS analysis indicates that both Sr and Cr are present in this submicron particle (Fig.6b). The chromium deposition at the lanthanum-containing cathodes can be semi-quantitatively determined. The overall content of Cr is 3.6 wt% and it is 18.2 wt% for Sr. This corresponds to an atomic ratio of  $\text{Sr}/\text{Cr} = 3:1$ . This indicates that segregated SrO particles have high affinity to the gaseous Cr species and Cr deposition is closely related to the segregated SrO on the LSCF surface.

The Cr deposition on Sr-rich particles is further confirmed on the LSCF bar sample after heat-treatment in the presence of  $\text{Cr}_2\text{O}_3$  in wet air at  $800^\circ\text{C}$  for 96 h. Figure 7 is the typical EDS layer image of segregated  $\text{SrO}_2$  particles on the LSCF surface. The size of the segregated Sr-rich particles is  $\sim 1 \mu\text{m}$ , bigger than that in dry air, most likely due to the accelerated Cr deposition in humidified air.<sup>45</sup> Both Sr and Cr were detected in the particles with 9.1 wt% of Cr and 16.4 wt% of Sr, corresponding to an atomic ratio of  $\text{Sr}/\text{Cr}=1.07:1$ , very close to the atomic ratio of  $\text{Sr}/\text{Cr}=1:1$  in  $\text{SrCrO}_4$ . The high content of Sr and Cr of the particle indicates the high activity between the segregated SrO particles and gaseous Cr species, leading to the

Cr deposition (Fig.7c). The observation of the formation of the Sr/Cr particles with Sr/Cr = 1 indicates the formation of SrCrO<sub>4</sub> phase as observed on porous LSCF cathodes.<sup>31, 52</sup>

### 3.3 Chemical reactivity between SrO, Co<sub>3</sub>O<sub>4</sub> and Cr<sub>2</sub>O<sub>3</sub>

The preferential deposition of Cr on the segregated SrO but not on the segregated Co<sub>3</sub>O<sub>4</sub> indicates that there may exist significant differences in the reactivity between SrO, Co<sub>3</sub>O<sub>4</sub> and Cr<sub>2</sub>O<sub>3</sub>. In order to further assess the reactivity between SrO, Co<sub>3</sub>O<sub>4</sub> and Cr<sub>2</sub>O<sub>3</sub>, various oxide couples of SrO-Co<sub>3</sub>O<sub>4</sub>-Cr<sub>2</sub>O<sub>3</sub> by solid state mixing method and by sol-gel solution mixing method were heat-treated at 800 °C for 2 h and the results are given in Fig.8 and Table 2. In the case of the binary oxide couples, reactions with each other occur at 800 °C and the reaction products were identified to be SrCrO<sub>4</sub>, CoCr<sub>2</sub>O<sub>4</sub>, and SrCoO<sub>3</sub>, respectively (Fig.8a). However, in the case of ternary SrO-Co<sub>3</sub>O<sub>4</sub>-Cr<sub>2</sub>O<sub>3</sub> oxide couples, the reactivity between these three oxides depends on the relative ratio of the oxides. In the case of the Cr-poor oxide couple, i.e., Sr:Co:Cr=1:1:0.25, Cr<sub>2</sub>O<sub>3</sub> completely reacted with SrO, forming SrCrO<sub>4</sub>. The remaining SrO reacted with cobalt oxide to form SrCoO<sub>3</sub>, and Co<sub>3</sub>O<sub>4</sub> was in excess (curve I in Fig.8b). No CoCr<sub>2</sub>O<sub>4</sub> was detected, implying that the reaction between Cr<sub>2</sub>O<sub>3</sub> and Co<sub>3</sub>O<sub>4</sub> is retarded in the presence of SrO. Instead, Co<sub>3</sub>O<sub>4</sub> reacted with SrO to form SrCoO<sub>3</sub>. This in turn implies that SrO is very active with Cr<sub>2</sub>O<sub>3</sub> to form the SrCrO<sub>4</sub> phase.

In the case of Cr-rich oxide couple, i.e., Sr:Co:Cr=1:1:4, SrO completely reacted with Cr<sub>2</sub>O<sub>3</sub>, forming SrCrO<sub>4</sub>. No CoCr<sub>2</sub>O<sub>4</sub> peak was observed despite the existence of

$\text{Co}_3\text{O}_4$  and  $\text{Cr}_2\text{O}_3$  in the mixture (curve II in Fig.8b). The formation of  $\text{SrCrO}_4$  rather than  $\text{CoCr}_2\text{O}_4$  in the case of  $\text{SrO-Co}_3\text{O}_4\text{-Cr}_2\text{O}_3$  oxide couples by solid state mixing method with high Cr content indicates that  $\text{Cr}_2\text{O}_3$  would selectively and preferentially react the SrO oxides and the presence of SrO retards the reaction between  $\text{Cr}_2\text{O}_3$  and  $\text{Co}_3\text{O}_4$ . However, very different from that by solid state mixing method, in the case of Cr-rich couple, Sr:Co:Cr=1:1:4 prepared by sol-gel solution mixing method, the formation of  $\text{SrCrO}_4$  as well as  $\text{CoCr}_2\text{O}_4$  phases was detected with excess of  $\text{Cr}_2\text{O}_3$  (Fig.8c). The only difference between the Sr-Co-Cr oxide couple by solid state oxide mixing and sol-gel solution mixing is that the Sr, Co and Cr would mix in molecule level in the sol-gel mixing method. This suggests that in the presence of SrO,  $\text{Cr}_2\text{O}_3$  could only be reactive with  $\text{Co}_3\text{O}_4$  to form  $\text{CoCr}_2\text{O}_4$  phase when cobalt and chromium precursors are mixed at the molecular level.

The exclusion of the activity between  $\text{Cr}_2\text{O}_3$  and  $\text{Co}_3\text{O}_4$  couple in the presence of SrO in the case of solid state mixing method appears to be a new phenomenon and such exclusion phenomenon is supported by the fact in the absence of SrO,  $\text{Co}_3\text{O}_4$  will react with  $\text{Cr}_2\text{O}_3$  to form  $\text{CoCr}_2\text{O}_4$  (Fig.8a). However, the reason for such exclusion phenomenon in oxide reaction activities is not clear at this stage.

#### *3.4. Selective and preferential Cr deposition*

Surface segregation in Sr doped lanthanum manganite and cobalt ferrite perovskites is a well-known phenomenon. Using angle-resolved x-ray photoelectron spectroscopy, electron energy loss spectroscopy and Auger electron spectroscopy, several independent studies have reported the evidences for Sr segregation on the

surface of LSM perovskites.<sup>60, 68-70</sup> Strontium and cobalt segregation is also reported for lanthanum cobaltite perovskites. Simner et al.<sup>63</sup> reported the segregation of SrO on the surface of LSCF after test in air at 750 °C using XPS. Vovk et al.<sup>71</sup> studied the  $\text{La}_{0.5}\text{Sr}_{0.5}\text{CoO}_3$  perovskite oxide surfaces under electrochemical polarization using *in situ* XPS technique. Under cathodic polarization, the Sr/(La+Co) ratio at the oxide surface increased irreversibly by 5% while the La/Co ratio remained constant, indicating the surface enrichment of strontium.

Using fully dense LSCF bar samples, SEM and EDS mapping analysis (Fig.2 and 3) of the present study clearly shows the segregation of SrO and  $\text{Co}_3\text{O}_4$  fine particles on the surface after annealing at 800 °C in air for 96 h. LSCF exhibits a substantial oxygen deficiency<sup>72</sup> and the presence of oxygen vacancies would reduce stability of the structure by weakening the attractive force. According to Oh et al.,<sup>59</sup> some cations near the surface will precipitate on the surface to reduce the excess surface energy caused by oxygen vacancy formation. In the case of LSCF segregation of A-site cation such as Sr is predominant. Our results also indicate the segregation of B-site cation such Co for LSCF samples annealed at 800°C. The formation of separated SrO and  $\text{Co}_3\text{O}_4$  particles indicates that both surface Sr and in particular Co species are quite mobile on the LSCF surface, similar to Mn species.<sup>73</sup> This is indicated by the formation of isolated and large  $\text{Co}_3\text{O}_4$  particles and more uniformly distributed submicron-sized SrO particles (Figs. 2 and 3).

In the presence of Cr source like  $\text{Cr}_2\text{O}_3$  used in the present study, high valence Cr gaseous species such as  $\text{CrO}_3$  in dry air and  $\text{CrO}_2(\text{OH})_2$  in wet air will be present over

the LSCF samples. Thus, Cr deposition and surface segregation of cations such as Sr and Co would occur simultaneously on the surface of LSCF. However, the observation of almost pure  $\text{Co}_3\text{O}_4$  and Sr-Cr particles with Sr/Cr ratio of 3:1 in dry air and 1:1 in wet air on the surface of LSCF in the presence of gaseous Cr species indicates that the presence of segregated SrO and/or the formation of  $\text{SrCrO}_4$  particles also retards the reaction between the gaseous Cr species and segregated  $\text{Co}_3\text{O}_4$  particles. This indicates that Cr deposition on LSCF is highly selective and preferentially takes place on the segregated SrO. Such selective and preferential deposition of Cr species on the surface of LSCF electrode materials is schematically illustrated in Fig.9. The fundamental reason for the selective and preferential Cr deposition on the segregated SrO is due to the exclusion effect of the presence of SrO on the reactivity between the gaseous Cr species and segregated  $\text{Co}_3\text{O}_4$ , consistent with the results of the oxide couple study. The significant grain growth of the Sr-rich particles on the LSCF surface in the presence of  $\text{Cr}_2\text{O}_3$  indicates that Cr interact or deposition on the SrO particles would also accelerate the Sr segregation from the LSCF perovskite lattice. The overall reaction between Cr species and segregated SrO particles can be written in general as follows based on the nucleation theory:<sup>31</sup>



Similar reaction can be written between for the reaction between  $\text{CrO}_2(\text{OH})_2$  and SrO.

Cobalt chromite spinels such as  $\text{CoCr}_2\text{O}_4$  are frequently used as catalysts for

catalytic combustion of methane.<sup>74, 75</sup> In fact, Gu et al. observed the formation of  $\text{CoCr}_2\text{O}_4$  on  $\text{NdBaCo}_2\text{O}_{5+\delta}$  electrode after annealing at  $800^\circ\text{C}$  for 2 h, where the electrode was in direct contact with a Cr pellet.<sup>76</sup> However, in the case of porous Sr and Co-containing perovskite electrodes such as LSCF, BSCF and  $(\text{La,Sr})(\text{MnCo})\text{O}_3$  cathodes, the dominant phase is  $\text{SrCrO}_4$  but not cobalt chromite.<sup>30, 31, 52, 77-79</sup> This again indicates that the inertness of segregated  $\text{Co}_3\text{O}_4$  toward Cr deposition is related to the exclusion effect of the presence of the segregated SrO on the activity of cobalt oxides towards Cr. The significantly high activity of segregated SrO as compared to that of  $\text{Co}_3\text{O}_4$  also implies that segregated SrO is a much better nucleation agent for the Cr deposition process.

## Conclusion

LSCF dense bar samples were used to study the relationship between the surface segregation and Cr deposition of LSCF cathode materials. SEM and FIB-EDS results indicate that both Sr and Co segregated on the LSCF surface and formed separated SrO and  $\text{Co}_3\text{O}_4$  oxide particles after annealing at  $800^\circ\text{C}$  in air for 96 h. In the presence of  $\text{Cr}_2\text{O}_3$  as gaseous Cr source, Cr deposition occurs preferentially on SrO particles, but in the case of segregated  $\text{Co}_3\text{O}_4$  particles, Cr deposition is negligible. The SrO- $\text{Co}_3\text{O}_4$ - $\text{Cr}_2\text{O}_3$  oxide couple study shows that the presence of SrO retards the reaction between  $\text{Cr}_2\text{O}_3$  and  $\text{Co}_3\text{O}_4$ , indicating the exclusion effect of the SrO on the reaction activity between  $\text{Cr}_2\text{O}_3$  and  $\text{Co}_3\text{O}_4$ . However, the exclusion effect of SrO diminishes when the oxide precursors were mixed in molecular level, e.g., by sol-gel

mixing method. This study provides the explicit evidences that Cr deposition is selective and preferential on the SrO segregated on the LSCF surface. The fundamental reason for the selective and preferential Cr deposition on segregated SrO is due to the exclusion effect of the presence of SrO on the reactivity between gaseous Cr species and segregated  $\text{Co}_3\text{O}_4$ , inhibiting the Cr deposition on the segregated  $\text{Co}_3\text{O}_4$  particles.

### Acknowledgements

The project is supported by Australian Research Council *Linkage Project funding scheme* (project number: LP110200281). The authors acknowledge the facilities, scientific and technical assistance of the University of Queensland, University of New South Wales and Curtin University Electron Microscope Centres and Laboratories, a facility partially funded by the University, State and Commonwealth Governments.

### References:

1. E. D. Wachsman and K. T. Lee, *Science*, 2011, **334**, 935-939.
2. D. J. L. Brett, A. Atkinson, N. P. Brandon and S. J. Skinner, *Chem. Soc. Rev.*, 2008, **37**, 1568-1578.
3. S. B. Adler, *Chem. Rev.*, 2004, **104**, 4791-4843.
4. N. Ai, S. P. Jiang, Z. Lu, K. F. Chen and W. H. Su, *J. Electrochem. Soc.*, 2010, **157**, B1033-B1039.
5. A. J. Samson, M. Sogaard and N. Bonanos, *Solid State Ionics*, 2012, **211**, 74-79.
6. B. K. Lai, K. Kerman and S. Ramanathan, *J. Power Sources*, 2011, **196**, 1826-1832.
7. S. P. Jiang, *Solid State Ionics*, 2002, **146**, 1-22.
8. A. Esquirol, N. P. Brandon, J. A. Kilner and M. Mogensen, *J. Electrochem. Soc.*, 2004, **151**, A1847-A1855.
9. C. S. Hsu and B. H. Hwang, *J. Electrochem. Soc.*, 2006, **153**, A1478-A1483.
10. J. A. Lane, S. J. Benson, D. Waller and J. A. Kilner, *Solid State Ionics*, 1999, **121**, 201-208.
11. S. R. Wang, T. Kato, S. Nagata, T. Honda, T. Kaneko, N. Iwashita and M. Dokiya, *Solid State Ionics*, 2002, **146**, 203-210.
12. Z. Liu, M. F. Han and W. T. Miao, *J. Power Sources*, 2007, **173**, 837-841.

13. J. M. Bae and B. C. H. Steele, *Solid State Ionics*, 1998, **106**, 247-253.
14. E. N. Armstrong, K. L. Duncan, D. J. Oh, J. F. Weaver and E. D. Wachsman, *J. Electrochem. Soc.*, 2011, **158**, B492-B499.
15. Y. X. Zhang and C. R. Xia, *Journal of Power Sources*, 2010, **195**, 6611-6618.
16. C. R. Xia, R. William, F. L. Chen and M. L. Liu, *Solid State Ionics*, 2002, **149**, 11-19.
17. S. McIntosh, J. F. Vente, W. G. Haije, D. H. A. Blank and H. J. M. Bouwmeester, *Chemistry of Materials*, 2006, **18**, 2187-2193.
18. K. Zhang, L. Ge, R. Ran, Z. Shao and S. Liu, *Acta Materialia*, 2008, **56**, 4876-4889.
19. J. W. Fergus, *Solid State Ionics*, 2004, **171**, 1-15.
20. J. W. Fergus, *Mater. Sci. Eng. A-Struct. Mater. Prop. Microstruct. Process.*, 2005, **397**, 271-283.
21. W. Z. Zhu and S. C. Deevi, *Mater. Sci. Eng. A-Struct. Mater. Prop. Microstruct. Process.*, 2003, **348**, 227-243.
22. B. Hua, J. Pu, J. F. Zhang, F. S. Lu, B. Chi and L. Jian, *J. Electrochem. Soc.*, 2009, **156**, B93-B98.
23. H. S. Seo, G. Jin, J. H. Jun, D.-H. Kim and K. Y. Kim, *Journal of Power Sources*, 2008, **178**, 1-8.
24. B. Hua, Y. H. Kong, W. Y. Zhang, J. Pu, B. Chi and L. Jian, *J. Power Sources*, 2011, **196**, 7627-7638.
25. K. Hilpert, D. Das, M. Miller, D. H. Peck and R. Weiss, *J. Electrochem. Soc.*, 1996, **143**, 3642-3647.
26. J. Froitzheim, H. Ravash, E. Larsson, L. G. Johansson and J. E. Svensson, *J. Electrochem. Soc.*, 2010, **157**, B1295-B1300.
27. S. C. Paulson and V. I. Birss, *J. Electrochem. Soc.*, 2004, **151**, A1961-A1968.
28. M. C. Tucker, H. Kurokawa, C. P. Jacobson, L. C. De Jonghe and S. J. Visco, *Journal of Power Sources*, 2006, **160**, 130-138.
29. Y. M. Kim, X. B. Chen, S. P. Jiang and J. Bae, *Electrochem. Solid State Lett.*, 2011, **14**, B41-B45.
30. Y. M. Kim, X. B. Chen, S. P. Jiang and J. Bae, *J. Electrochem. Soc.*, 2012, **159**, B185-B194.
31. S. P. Jiang, S. Zhang and Y. D. Zhen, *J. Electrochem. Soc.*, 2006, **153**, A127-A134.
32. S. N. Lee, A. Atkinson and J. A. Kilner, *J. Electrochem. Soc.*, 2013, **160**, F629-F635.
33. X. B. Chen, B. Hua, J. Pu, J. Li, L. Zhang and S. P. Jiang, *Int. J. Hydrog. Energy*, 2009, **34**, 5737-5748.
34. Y. D. Zhen, A. I. Y. Tok, F. Y. C. Boey and S. P. Jiang, *Electrochem. Solid State Lett.*, 2008, **11**, B42-B46.
35. X. B. Chen and S. P. Jiang, *Journal of Materials Chemistry A*, 2013, **1**, 4871-4878.
36. S. P. Jiang and X. B. Chen, *Int. J. Hydrog. Energy*, 2014, **39**, 505-531.
37. S. P. S. Badwal, R. Deller, K. Foger, Y. Ramprakash and J. P. Zhang, *Solid State Ionics*, 1997, **99**, 297-310.
38. S. Taniguchi, M. Kadowaki, H. Kawamura, T. Yasuo, Y. Akiyama, Y. Miyake and T. Saitoh, *J. Power Sources*, 1995, **55**, 73-79.
39. Y. Matsuzaki and I. Yasuda, *Solid State Ionics*, 2000, **132**, 271-278.
40. Y. Matsuzaki and I. Yasuda, *J. Electrochem. Soc.*, 2001, **148**, A126-A131.
41. T. Horita, Y. P. Xiong, H. Kishimoto, K. Yamaji, M. E. Brito and H. Yokokawa, *J. Electrochem. Soc.*, 2010, **157**, B614-B620.
42. M. Krumpelt, T. A. Cruse, B. J. Ingram, J. L. Routbort, S. L. Wang, P. A. Salvador and G. Chen, *J. Electrochem. Soc.*, 2010, **157**, B228-B233.
43. S. P. Jiang, J. P. Zhang, L. Apateanu and K. Foger, *J. Electrochem. Soc.*, 2000, **147**, 4013-4022.
44. S. P. Jiang, S. Zhang and Y. D. Zhen, *J. Mater. Res.*, 2005, **20**, 747-758.
45. X. B. Chen, Y. D. Zhen, J. Li and S. P. Jiang, *Int. J. Hydrog. Energy*, 2010, **35**, 2477-2485.
46. S. P. Jiang, Y. D. Zhen and S. Zhang, *J. Electrochem. Soc.*, 2006, **153**, A1511-A1517.
47. S. P. Jiang, J. P. Zhang and X. G. Zheng, *J. Eur. Ceram. Soc.*, 2002, **22**, 361-373.

48. X. B. Chen, L. Zhang and S. P. Jiang, *J. Electrochem. Soc.*, 2008, **155**, B1093-B1101.
49. Y. Zhen and S. P. Jiang, *J. Power Sources*, 2008, **180**, 695-703.
50. K. Wang and J. W. Fergus, *Electrochem. Solid State Lett.*, 2008, **11**, B156-B160.
51. S. P. Jiang, J. P. Zhang and K. Foger, *J. Electrochem. Soc.*, 2001, **148**, C447-C455.
52. E. Konyshcheva, H. Penkalla, E. Wessel, J. Mertens, U. Seeling, L. Singheiser and K. Hilpert, *J. Electrochem. Soc.*, 2006, **153**, A765-A773.
53. L. Zhao, J. Drennan, C. Kong, S. Amarasinghe and S. P. Jiang, *ECS Transactions*, 2013, **57**, 599-604.
54. G. C. Kostoglouidis and C. Ftikos, *Solid State Ionics*, 1999, **126**, 143-151.
55. D. Waller, J. A. Lane, J. A. Kilner and B. C. H. Steele, *Materials Letters*, 1996, **27**, 225-228.
56. A. Mineshige, J. Izutsu, M. Nakamura, K. Nigaki, J. Abe, M. Kobune, S. Fujii and T. Yazawa, *Solid State Ionics*, 2005, **176**, 1145-1149.
57. W. Zhou, R. Ran, Z. Shao, W. Zhuang, J. Jia, H. Gu, W. Jin and N. Xu, *Acta Materialia*, 2008, **56**, 2687-2698.
58. J. S. Hardy, J. W. Templeton, D. J. Edwards, Z. G. Lu and J. W. Stevenson, *J. Power Sources*, 2012, **198**, 76-82.
59. D. Oh, D. Gostovic and E. D. Wachsman, *J. Mater. Res.*, 2012, **27**, 1992-1999.
60. M. P. de Jong, V. A. Dediou, C. Taliani and W. R. Salaneck, *J. Appl. Phys.*, 2003, **94**, 7292-7296.
61. Q. H. Wu, M. L. Liu and W. Jaegermann, *Mater. Lett.*, 2005, **59**, 1480-1483.
62. Z. H. Cai, M. Kubicek, J. Fleig and B. Yildiz, *Chem. Mat.*, 2012, **24**, 1116-1127.
63. S. P. Simner, M. D. Anderson, M. H. Engelhard and J. W. Stevenson, *Electrochemical and Solid-State Letters*, 2006, **9**, A478-A481.
64. F. S. Baumann, J. r. Fleig, M. Konuma, U. Starke, H.-U. Habermeier and J. Maier, *Journal of The Electrochemical Society*, 2005, **152**, A2074-A2079.
65. M. Liu, D. Ding, K. Blinn, X. Li, L. Nie and M. Liu, *International Journal of Hydrogen Energy*, 2012, **37**, 8613-8620.
66. S. B. Tan, Q. H. Yang and Z. C. Zhang, *Acta Polym. Sin.*, 2010, 1269-1275.
67. L. Zhao, J. Zhang, T. Becker and S. P. Jiang, *J. Electrochem. Soc.*, 2014, **161**, F687-F693.
68. Q. H. Wu, M. L. Liu and W. Jaegermann, *Mater. Lett.*, 2005, **59**, 1980-1983.
69. H. Dulli, P. A. Dowben, S. H. Liou and E. W. Plummer, *Phys. Rev. B*, 2000, **62**, 14629-14632.
70. K. Katsiev, B. Yildiz, K. Balasubramaniam and P. A. Salvador, *Appl. Phys. Lett.*, 2009, **95**, 92106.
71. G. Vovk, X. Chen and C. A. Mims, *Journal of Physical Chemistry B*, 2005, **109**, 2445-2454.
72. L. W. Tai, M. M. Nasrallah, H. U. Anderson, D. M. Sparlin and S. R. Sehlin, *Solid State Ionics*, 1995, **76**, 273-283.
73. M. Backhaus-Ricoult, K. Adib, T. S. Clair, B. Luerssen, L. Gregoratti and A. Barinov, *Solid State Ionics*, 2008, **179**, 891-895.
74. J. H. Chen, X. Y. Zhang, H. Arandiyani, Y. Peng, H. Z. Chang and J. H. Li, *Catal. Today*, 2013, **201**, 12-18.
75. D. Fino, S. Solaro, N. Russo, G. Saracco and V. Specchia, *Top. Catal.*, 2007, **42-43**, 449-454.
76. H. T. Gu, H. Chen, Y. F. Zheng and L. C. Guo, *Int. J. Hydrog. Energy*, 2010, **35**, 2457-2462.
77. X. B. Chen, L. Zhang, E. J. Liu and S. P. Jiang, *Int. J. Hydrog. Energy*, 2011, **36**, 805-821.
78. S. P. Simner, M. D. Anderson, G. G. Xia, Z. Yang, L. R. Pederson and J. W. Stevenson, *J. Electrochem. Soc.*, 2005, **152**, A740-A745.
79. M. R. Ardigo, A. Perron, L. Combemale, O. Heintz, G. Caboche and S. Chevalier, *J. Power Sources*, 2011, **196**, 2037-2045.

**Figure Captions:**

1. XRD diffraction patterns of LSCF bar samples; (a) freshly-prepared, (b) heat-treated at 800 °C in dry air for 96 h, (c) heat-treated in the presence of Cr<sub>2</sub>O<sub>3</sub> at 800 °C in dry air for 96 h, and (d) heat-treated in the presence of Cr<sub>2</sub>O<sub>3</sub> at 800 °C in wet air for 96 h.
2. SEM micrographs of (a,b) the freshly-prepared LSCF and (c,d) LSCF samples after heat treated at 800 °C in the absence of Cr<sub>2</sub>O<sub>3</sub> in air for 96 h; (e) enlarged image of the segregated micron-sized particle as circled in (d); and (f) typical EDS spectrum of LSCF grains in (b). Arrows in (d) indicate segregated isolated submicron-sized particles.
3. SEM micrographs of LSCF surface after (a) heat-treated at 800 °C in dry air for 96 h (b) heat-treated in the presence of Cr<sub>2</sub>O<sub>3</sub> at 800 °C in dry air for 96 h, (c) heat-treated in the presence of Cr<sub>2</sub>O<sub>3</sub> at 800 °C in wet air for 96 h, and (d) freshly prepared.
4. SEM micrographs of LSCF surface after heat-treated at 800 °C in the presence of Cr<sub>2</sub>O<sub>3</sub> (a) in dry air for 96 h and (b) in wet air for 96 h,
5. (a) EDS layered electron image, (b) EDS spectrum and (c) FIB-EDS mapping of typical Co-rich particles on LSCF surface after heat-treatment in the presence of Cr<sub>2</sub>O<sub>3</sub> and dry air at 800 °C for 96 h.
6. (a) EDS layered electron image, (b) EDS spectrum and (c) FIB-EDS mapping of typical submicron Sr-rich particle on LSCF surface after heat-treatment in the presence of Cr<sub>2</sub>O<sub>3</sub> and dry air at 800 °C for 96 h. The Sr- and Cr-rich

- regions are indicated by a circle.
- (a) EDS layered electron image, (b) EDS spectrum and (c) FIB-EDS mapping of typical submicron Sr-rich particle on LSCF surface after heat-treatment in the presence of  $\text{Cr}_2\text{O}_3$  and wet air at 800 °C for 96 h. The Sr- and Cr-rich regions are indicated by a circle.
  - XRD diffraction patterns of (a) binary oxide couples by solid state oxide mixture; (I)  $\text{SrO-Cr}_2\text{O}_3$  with Sr:Cr=1:1, (II)  $\text{Co}_3\text{O}_4\text{-Cr}_2\text{O}_3$  with Co:Cr=1:1, (III)  $\text{SrO-Co}_3\text{O}_4$  with Sr:Co=1:1, (b) ternary oxide couples by solid state oxide mixture; (I)  $\text{SrO-Co}_3\text{O}_4\text{-Cr}_2\text{O}_3$  with Sr:Co:Cr=1:1:0.25, (II)  $\text{SrO-Co}_3\text{O}_4\text{-Cr}_2\text{O}_3$  with Sr:Co:Cr=1:1:4, and (c)  $\text{SrO-Co}_3\text{O}_4\text{-Cr}_2\text{O}_3$  with Sr:Co:Cr=1:1:4 by sol-gel solution mixture. All oxide couples were calcination at 800 °C for 2 h.
  - Scheme of (a) segregation and formation of  $\text{Co}_3\text{O}_4$  and SrO and (b) the selective and preferential deposition and reaction of Cr species with segregated SrO on the surface of LSCF electrode material.

**Table 1.** Lattice parameters of rhombohedral  $\text{La}_{0.6}\text{Sr}_{0.4}\text{Co}_{0.2}\text{Fe}_{0.8}\text{O}_{3-\delta}$  perovskite bar samples.

$\text{La}_{0.6}\text{Sr}_{0.4}\text{Co}_{0.2}\text{Fe}_{0.8}\text{O}_{3-\delta}$	$a$ (Å)	$c$ (Å)	$V$ (Å) <sup>3</sup>
Freshly-prepared (a)	5.493	13.32	348.0
Dry air without $\text{Cr}_2\text{O}_3$ (b)	5.493	13.37	349.4
Dry air with $\text{Cr}_2\text{O}_3$ (c)	5.502	13.38	350.8
Wet air with $\text{Cr}_2\text{O}_3$ (d)	5.502	13.35	350.0
Ref <sup>54</sup> freshly-prepared	5.492	13.36	349.1
Ref <sup>55</sup> freshly-prepared	5.496	13.34	349.1

**Table 2.** Reaction products of oxide couples heat-treated at 800°C in air for 2 h. “✓” presents the phases of products, “✗” indicates that the phase is not detected, and “-” indicates that the phases can’t be present in this case.

Oxide couples	Products					
	$\text{SrCrO}_4$	$\text{CoCr}_2\text{O}_4$	$\text{SrCoO}_3$	$\text{Cr}_2\text{O}_3$	$\text{SrO}$	$\text{Co}_3\text{O}_4$
Oxide couples by solid state mixing method						
SrO- $\text{Cr}_2\text{O}_3$ (Sr:Cr=1:1)	✓	-	-	✓	✗	-
$\text{Co}_3\text{O}_4$ - $\text{Cr}_2\text{O}_3$ (Co:Cr=1:1)	-	✓	-	✗	-	✓
SrO- $\text{Co}_3\text{O}_4$ (Sr:Co=1:1)	-	-	✓	-	✗	✓
SrO- $\text{Co}_3\text{O}_4$ - $\text{Cr}_2\text{O}_3$ (Sr:Co:Cr=1:1:0.25)	✓	✗	✓	✗	✗	✓
SrO- $\text{Co}_3\text{O}_4$ - $\text{Cr}_2\text{O}_3$ (Sr:Co:Cr=1:1:4)	✓	✗	✗	✓	✗	✓
Oxide couples by sol-gel solution mixing method						
SrO- $\text{Co}_3\text{O}_4$ - $\text{Cr}_2\text{O}_3$ (Sr:Co:Cr=1:1:4)	✓	✓	✗	✓	✗	✗

Figure 1

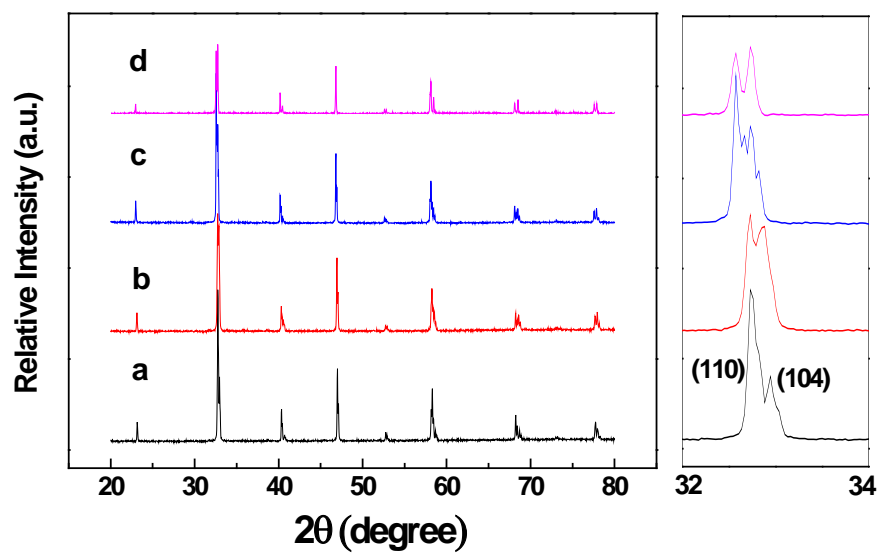


Figure 2

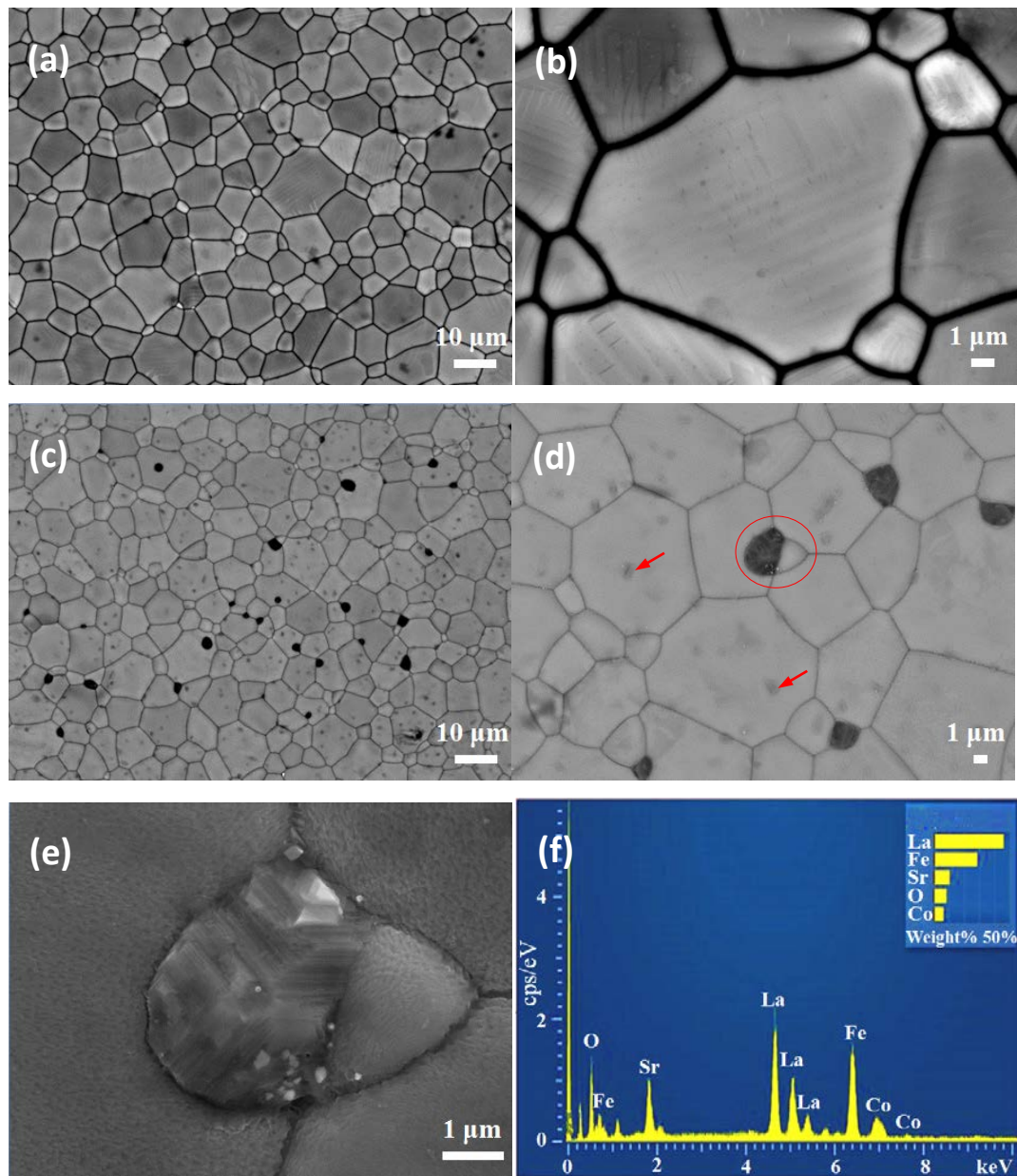


Figure 3

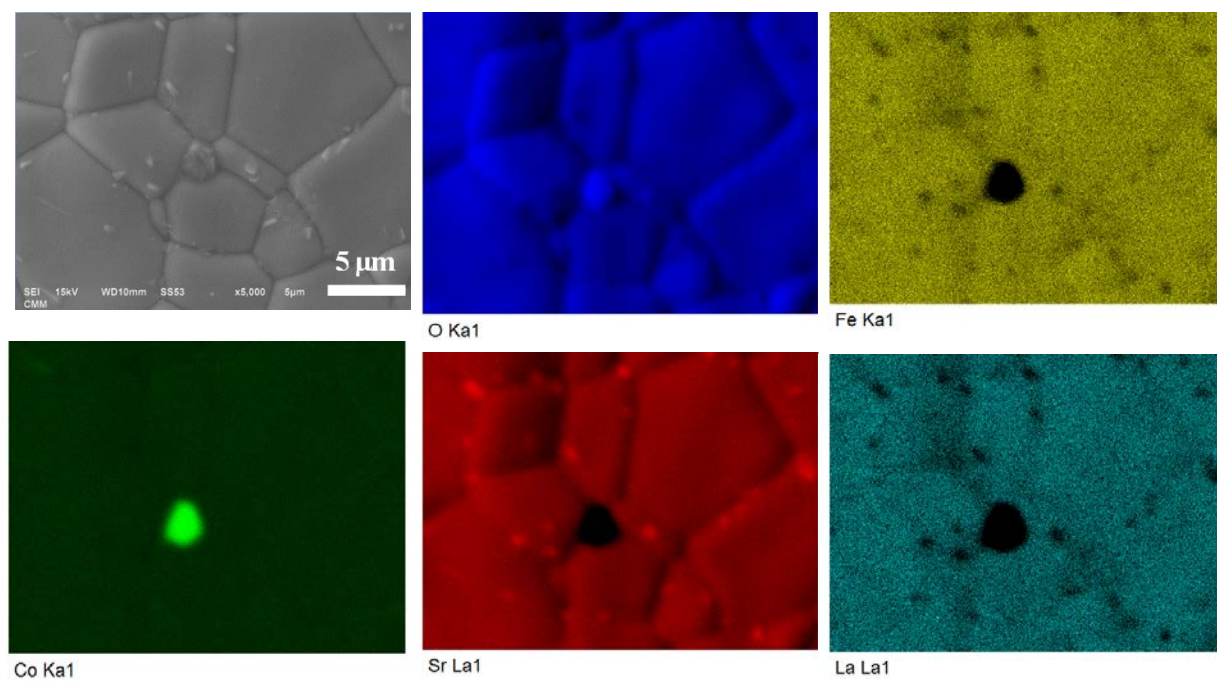


Figure 4

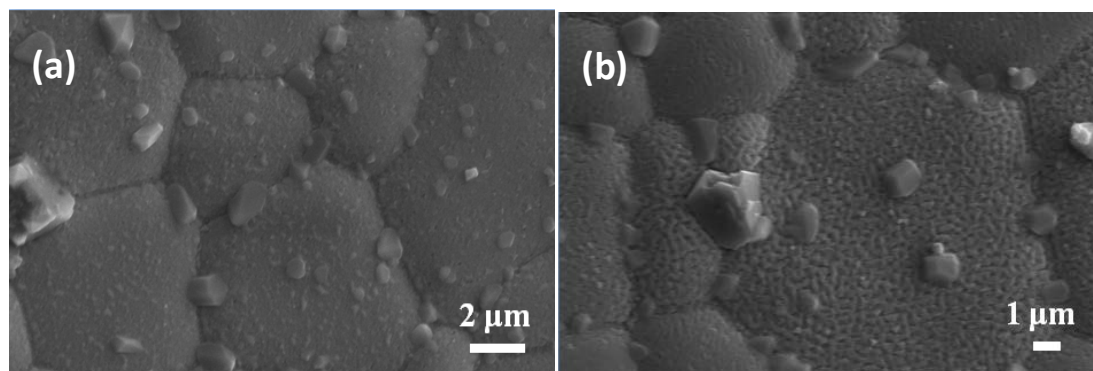


Figure 5

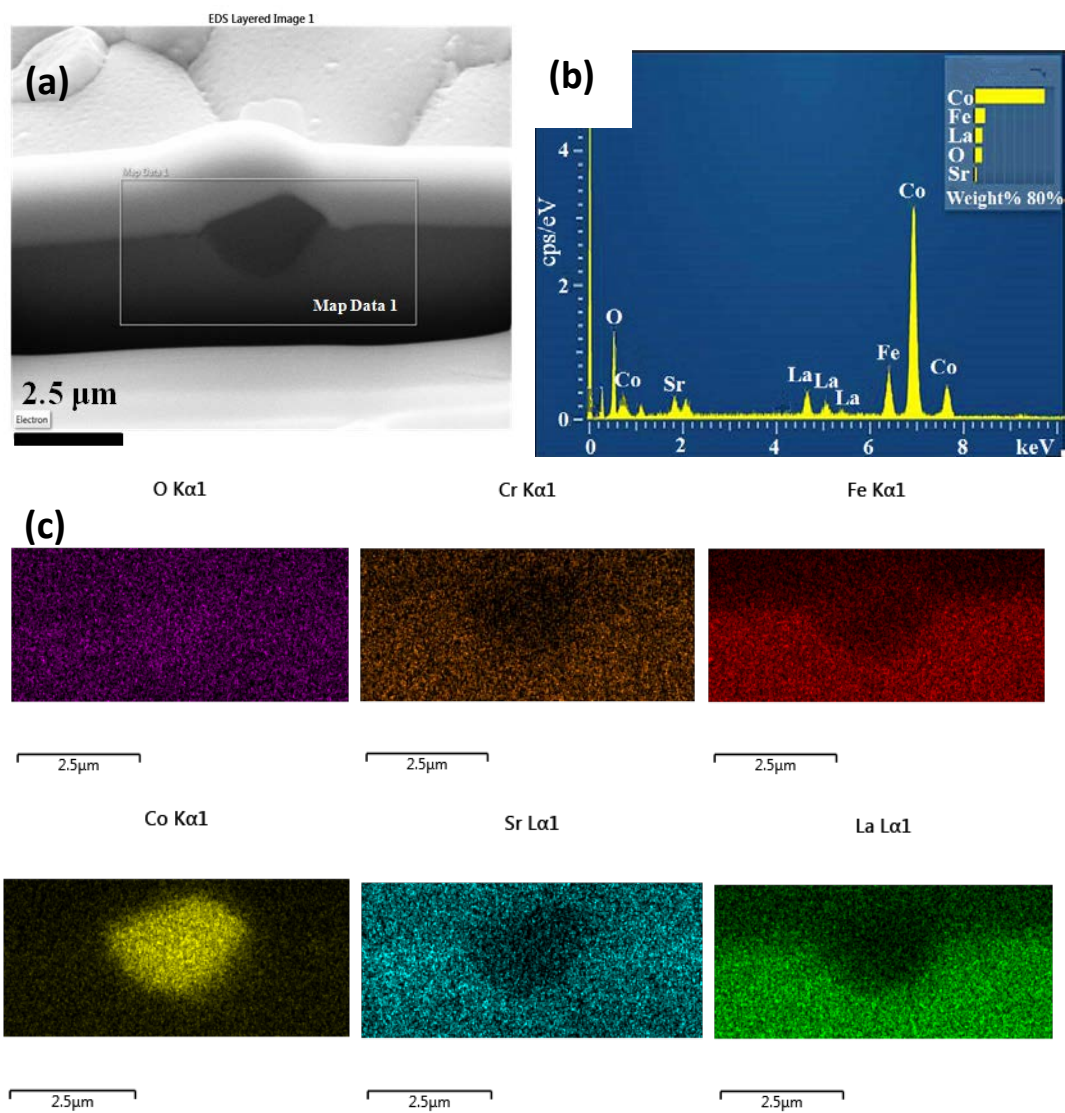


Figure 6

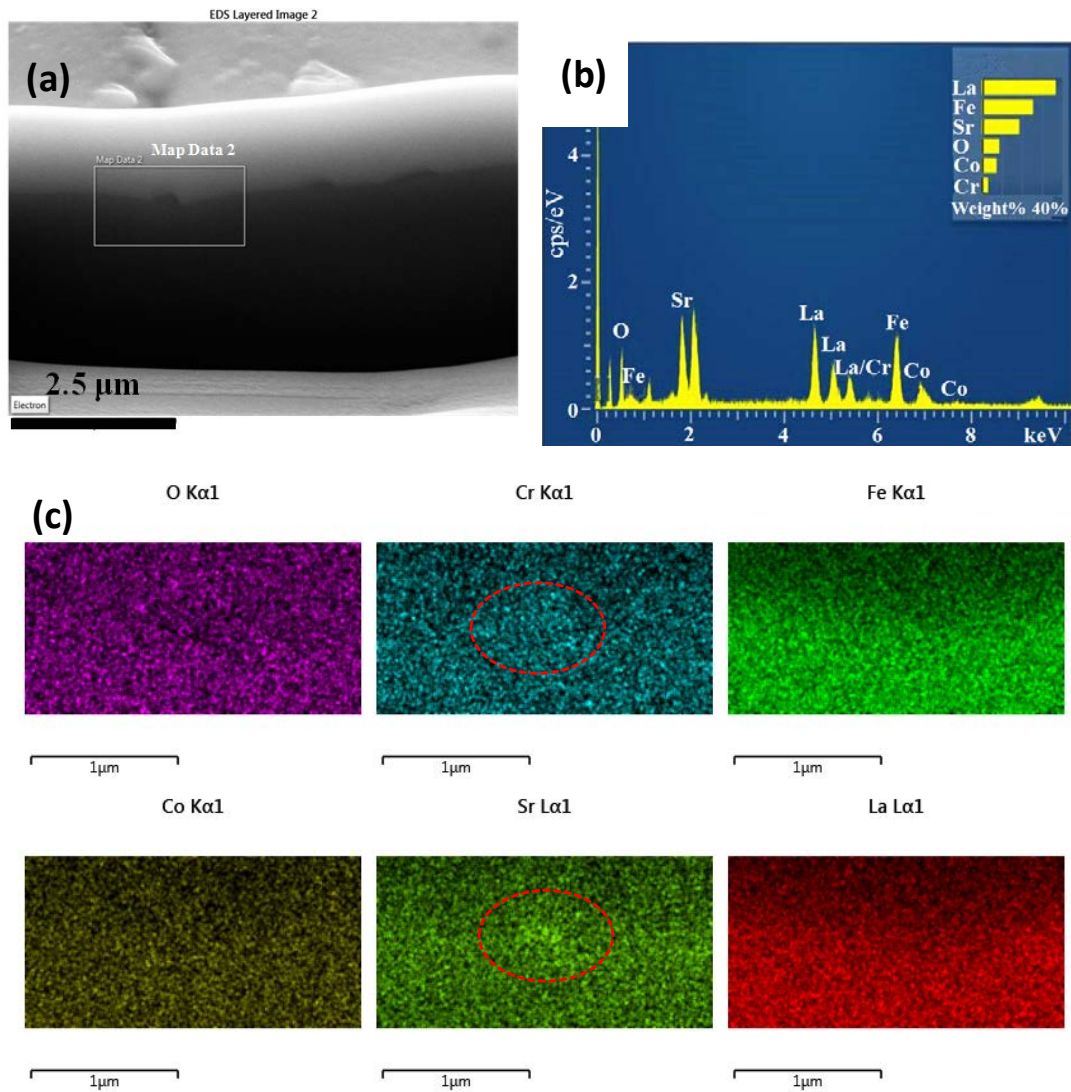


Figure 7

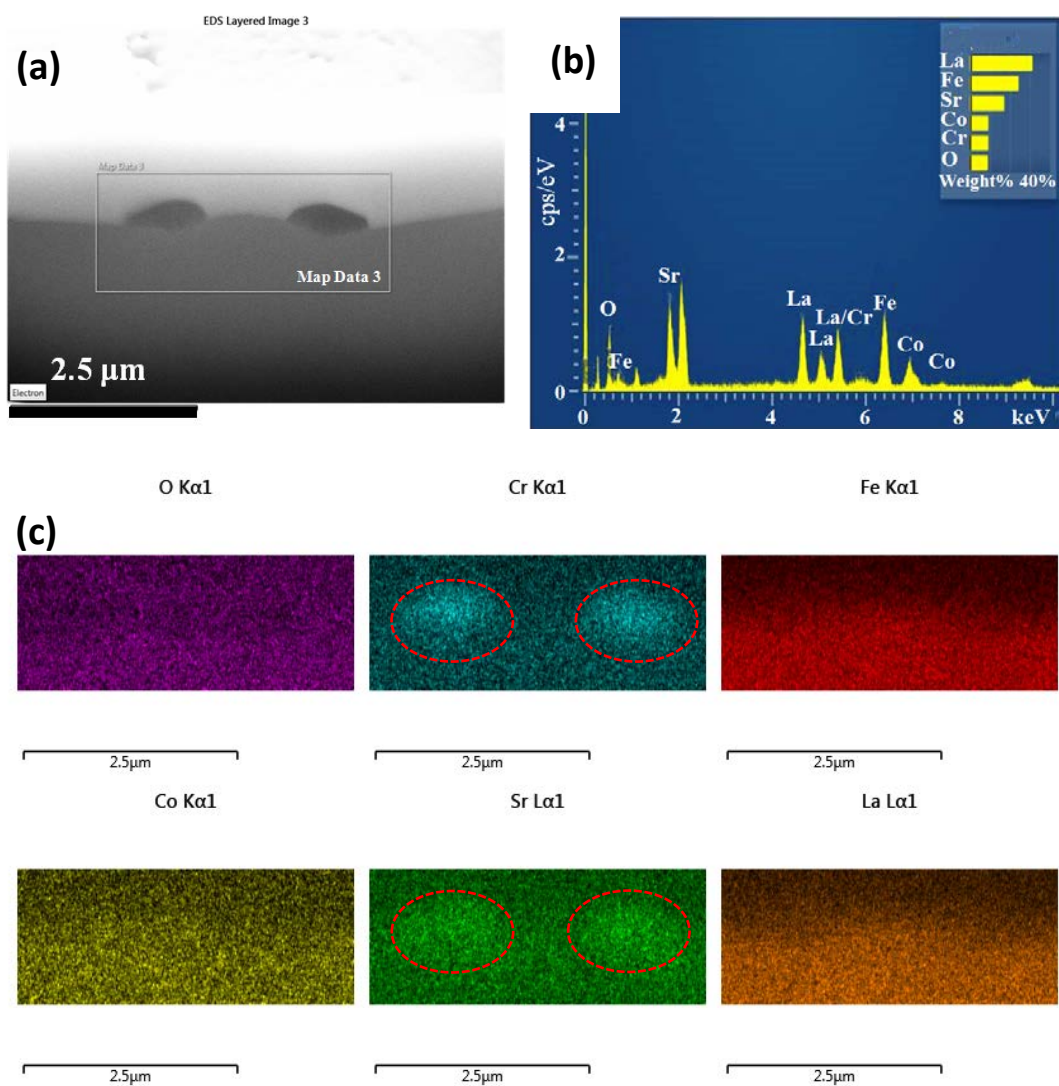


Figure 8

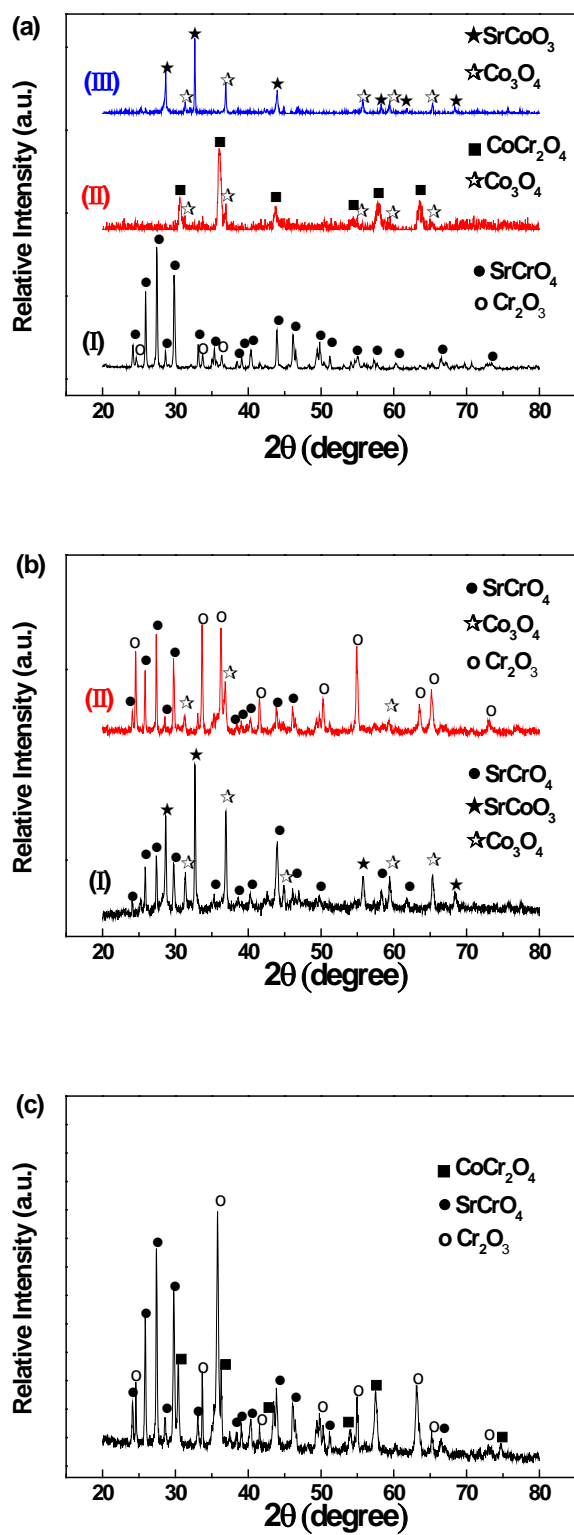


Figure 9

